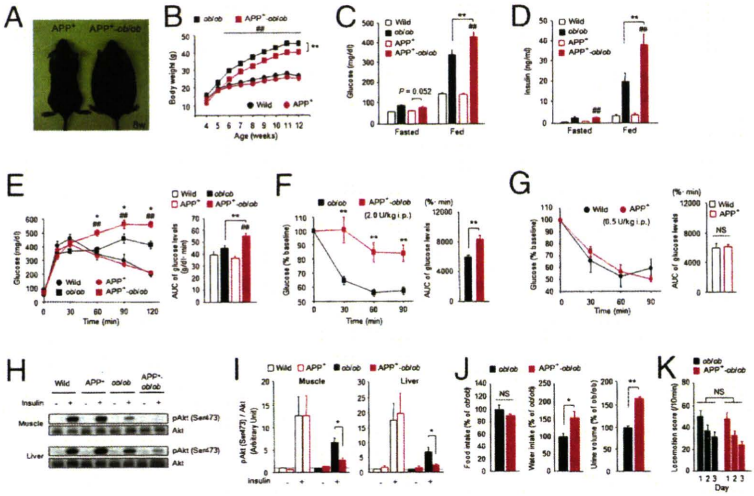

**Fig. 1.** Metabolic features of APP$^+$-*ob/ob* mice. (*A*) Appearance of APP$^+$ and APP$^+$-*ob/ob* mice at 8 weeks. (*B*) Body weight changes in WT, APP$^+$, *ob/ob*, and APP$^+$-*ob/ob* mice ($n$ = 12–14 per group). Blood glucose levels (*C*) and plasma insulin concentrations (*D*) at 8 weeks of age ($n$ = 5–9). (*E*) Blood glucose levels during glucose tolerance test at 8 weeks ($n$ = 5–14) and AUCs of blood glucose (*Right*) during GTT. (*F* and *G*) ITT in *ob/ob* and APP$^+$-*ob/ob* mice (2.0 U/kg, $n$ = 13–17, *F*), and WT and APP$^+$ mice (0.5 U/kg, $n$ = 5–6; *G*) at 8 weeks. (*H*) Immunoblot analysis of Ser473-phosphorylated Akt (pAkt) and total Akt in response to a bolus injection of insulin in skeletal muscle and liver. (*I*) Densitometric quantification of all immunoblot analysis from *H* ($n$ = 3–7). (*J*) Daily food (*Left*) and water (*Middle*) intake and urine volume (*Right*) in *ob/ob* and APP$^+$-*ob/ob* mice at 8 weeks ($n$ = 7–9). (*K*) Basal activity (mean locomotion score) of *ob/ob* and APP$^+$-*ob/ob* mice in open-field test ($n$ = 6–9). $^{\#\#}P <$ 0.01, APP$^+$-*ob/ob* versus APP$^+$ mice; $^*P < 0.05$ and $^{**}P < 0.01$, APP$^+$-*ob/ob* versus *ob/ob* mice. NS, not significant.

1*K*), although APP$^+$-*ob/ob* mice showed increased water intake (Fig. 1*J*) to compensate for water loss caused by glycosuria (Fig. 1*J*). These findings suggest that the pathological conditions accompanying AD may aggravate the severity of diabetes.

**Early Onset of Learning Deficit in APP$^+$-*ob/ob* Mice.** To assess whether a diabetic condition affects cognitive function, we performed the Morris water maze test. At the early age of 8 weeks, APP$^+$-*ob/ob* mice showed severe learning deficit in the hidden-platform test whereas APP$^+$ mice did not exhibit learning impairment (Fig. 2*A*). We also confirmed that *ob/ob* mice showed normal learning at this age (Fig. 2*A*). In the probe test, although APP$^+$ and *ob/ob* mice searched preferentially in the trained quadrant (Fig. 2*D*) and crossed over the previous platform location at levels comparable to those in WT mice (Fig. 2*C*), only APP$^+$-*ob/ob* mice showed significantly poor performance (Fig. 2 *C* and *D*). In the visible-platform test, there was no significant difference in escape latency among all groups (Fig. 2*B*), indicating that visual function did not differ among them. Difference in body weight itself could not have affected learning ability and performance in the test, because *ob/ob* mice (which gained more body weight than APP$^+$-*ob/ob* mice; Fig. 1*B*) showed normal learning in these tests (Fig. 2 *A–D*).

At 12 weeks of age, the severe learning deficit in APP$^+$-*ob/ob* mice was sustained, although APP$^+$ mice showed mild learning impairment (Fig. 2*E*). Notably, at this age, APP$^+$-*ob/ob* mice displayed an atypical pattern of performance in the visible-platform test (Fig. 2*F*), in which they performed poorly only in the early phase of the test (sessions 1 and 2), suggesting emotional disturbance in these mice. This impaired performance of APP$^+$-*ob/ob* mice reflected neither visual dysfunction nor poor swimming ability caused by obesity, because they performed well in the later phase of the test (Fig. 2*F*), and *ob/ob* mice showed nearly normal performance throughout the sessions (Fig. 2*F*). Emotional alterations associated with dementia (so-called behavioral and psychological symptoms of dementia) are also common problems in clinical practice. It is noteworthy that a diabetic condition exacerbated behavior reminiscent of behavioral and psychological symptoms of dementia in the AD mouse model.

To examine whether the impaired cognitive function in APP$^+$-*ob/ob* mice might be related to an increase in Aβ load in the brain, Aβ content in the brain-soluble and -insoluble fractions was quantified. Although the levels of Aβ40 and Aβ42 in APP$^+$ and APP$^+$-*ob/ob* mouse brain were significantly higher than those in APP transgene negative mice, no significant difference was observed between APP$^+$ and APP$^+$-*ob/ob* mice (Fig. 2 *G* and *H*). In this early stage of disease (12 weeks), no obvious amyloid plaque was detected in the brain of either group (Fig. 2*I*). Therefore, the exacerbation of cognitive impairment in APP$^+$-*ob/ob* mice might not be caused by an increase in brain Aβ burden.

**Effects of Diabetic Symptoms on Brain Pathology in APP$^+$-*ob/ob* Mice.** At 12 months of age, the brain weight of APP$^+$-*ob/ob* mice was significantly decreased compared with that in mice with other genotypes (Fig. S2*A*), suggesting that some kind of degenerative

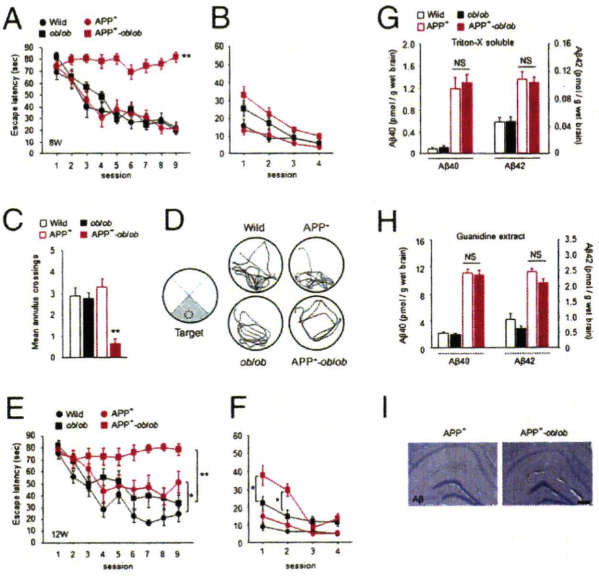

**Fig. 2.** Exacerbation of learning and memory deficit in APP$^+$-*ob/ob* mice, without increase in brain Aβ load. (*A–D*) Morris water maze test at 8 weeks. Escape latencies in hidden-platform (*A*) and visible-platform (*B*) test, number of annulus crossings (*C*), and representative swim paths (*D*) during the probe test are shown ($n$ = 11–17 per group). $^{**}P < 0.01$ for APP$^+$-*ob/ob* mice versus other genotypes. "Target" indicates the area where the platform was constantly located in the hidden-platform test. (*E* and *F*) Morris water maze test at 12 weeks. Escape latencies in hidden-platform (*E*) and visible-platform (*F*) test ($n$ = 11–13). $^*P < 0.05$, $^{**}P < 0.01$. (*G* and *H*) Quantification of brain Aβ40 and Aβ42 concentrations. Both Triton-X–soluble (*G*) and -insoluble (guanidine extract) (*H*) Aβ were measured ($n$ = 6–7). (*I*) Aβ immunostaining (6E10) in brain of APP$^+$ and APP$^+$-*ob/ob* mice. There was no detectable amyloid plaque at this early age (12 weeks) in either genotype. (Scale bar, 200 μm.)

changes had occurred in the brain. At this age, amyloid plaques had not developed in the hippocampus of either APP$^+$ or APP$^+$-*ob/ob* mice (Fig. S2*B Left*), whereas only faint amyloid plaques were seen in the entorhinal cortex (Fig. S2*B Right*). We quantified brain Aβ levels at this time point and found no significant difference between APP$^+$ and APP$^+$-*ob/ob* mice (Fig. S2*C*).

Many patients with AD present with cerebrovascular Aβ deposition (i.e., cerebral amyloid angiopathy), another pathological marker of this disease (17). Given the high prevalence of vascular complications in DM (18), severe pathological changes in the cerebral vasculature could be detected in APP$^+$-*ob/ob* mice and potentially impact on cognitive function. Thus, we isolated the microvessels from mouse brains (19) and immunostained them with anti-Aβ40 antibody. At 12 months of age, faint amyloid deposits had appeared in blood vessels in the brain of APP$^+$ mice (Fig. 3*A*). In APP$^+$-*ob/ob* mice, dense amyloid deposits were observed in small arteries (Fig. 3*A Upper*) as well as in arterioles and capillaries (Fig. 3*A Lower*). Different from the whole-brain Aβ level, the amount of Aβ40 in these isolated microvessels was significantly increased in APP$^+$-*ob/ob* mice compared with APP$^+$ mice (Fig. 3*B*), consistent with the immunohistochemical data.

This cerebrovascular amyloid deposition was age-dependent and appeared after 6 months of age in APP$^+$-*ob/ob* mice (Fig. 3*C*). As recent studies demonstrated that RAGE, which is well known to play an important role in the pathogenesis of diabetes (12), bound to soluble Aβ and mediated pathophysiologically relevant cellular responses in AD (13, 14), we focused on RAGE in the cerebral vasculature. At 3 months of age, even before the development of amyloid deposition in the cerebral vasculature, RAGE immunoreactivity was markedly increased in blood vessels of the APP$^+$-*ob/ob* mouse brain (Fig. 3*D*). Up-regulation of RAGE was relatively limited to the blood vessels labeled for CD31 (Fig. 3*E*), whereas no obvious signals were detected in neuronal cells (pyramidal cell layer of hippocampus, Fig. 3*E*). As the activation of RAGE induced a potent inflammatory response (13, 14), we examined the induction of inflammatory markers in the brain. Using immunostaining, a significant increase in IL-6 (Fig. 3*F*) and TNF-α (Fig. S3) was observed in the brain microvessels of APP$^+$-*ob/ob* mice compared with other genotypes.

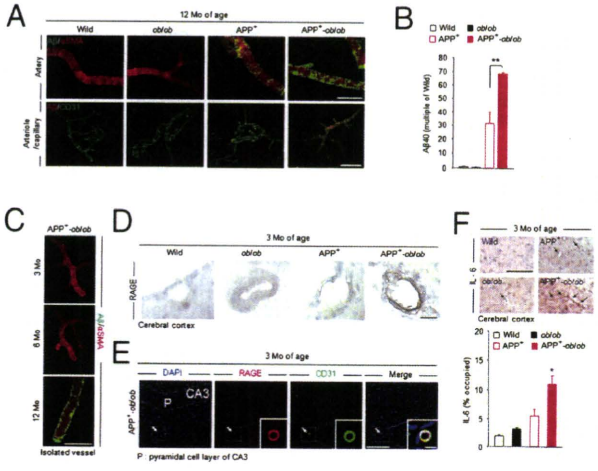


**Fig. 3.** Increased vascular amyloid deposition and inflammation in APP$^+$-*ob/ob* mouse brain. (*A*) Immunohistochemical detection of Aβ40 deposition in isolated brain microvessels of 12-month-old mice. Brain microvessels were also stained for anti–α-smooth muscle actin (a vascular smooth muscle cell marker) and CD31 (endothelial cell marker). (Scale bar, 100 μm.) (*B*) Quantification of Aβ40 level in isolated brain microvessels by ELISA ($n$ = 3 per group). $^{**}P < 0.01$. (*C*) Cerebrovascular amyloid deposition in APP$^+$-*ob/ob* mice was age-dependent and appeared after 6 months of age. (Scale bar, 100 μm.) (*D*) Immunohistochemical staining for RAGE in brain sections of young (3-month-old) mice. Strong immunoreactivity was detected in brain vessels (cerebral cortex) of APP$^+$-*ob/ob* mice. (Scale bar, 30 μm.) (*E*) Brain section of 3-month-old APP$^+$-*ob/ob* mouse immunolabeled for RAGE and CD31 and counterstained with DAPI. Colocalization of RAGE and CD31 in cerebral vessel is denoted by arrow and magnified (*Inset*). (Scale bars, 100 μm; 10 μm for *Inset*.) (*F*) IL-6–positive microvessels (cerebral cortex) in 3-month-old mouse (*Left*) and quantitative image analysis of IL-6–positive vessels (percent occupied; *Right*, $n$ = 3). (Scale bar, 100 μm.) $^{*}P < 0.05$ for APP$^+$-*ob/ob* mice versus other genotypes.

To assess reactive astrogliosis, we quantified the immunoreactivity of GFAP in the hippocampal area. Although APP$^+$ mice showed increased GFAP burden compared with WT mice, APP$^+$-*ob/ob* mice exhibited more marked reactive astrogliosis (Fig. S4*A*). Furthermore, we quantified choline acetyltransferase (ChAT)–immunoreactive fibers (i.e., cholinergic fibers) in the hippocampus. Aged APP$^+$-*ob/ob* mice exhibited a significant decrease in cholinergic nerve fibers compared with other genotypes (Fig. S4*B*).

To analyze the underlying mechanisms of these degenerative pathological changes, we investigated neuronal insulin signaling. Recently, it has been shown that insulin signaling plays an important role in synapse formation and regeneration of neurons in the brain (20). First, we quantified the amount of brain insulin by ELISA and found that brain insulin level was markedly decreased in APP$^+$-*ob/ob* mice compared with other genotypes (Fig. 4*A*). We also assessed the insulin sensitivity in brain neurons using an in vivo insulin stimulation assay (21). Although insulin stimulated formation of phosphatidylinositol 3,4,5-triphosphate (PIP3)—a major downstream marker of insulin signaling—in the arcuate nucleus of WT mice, the number of PIP3-positive cells was significantly decreased in APP$^+$-*ob/ob* mice compared with APP$^+$ mice and ob/ob mice (Fig. 4*B*). We also examined insulin stimulated Akt phosphorylation (Ser473) in the brain (hypothalamus), and found that Akt phosphorylation was significantly suppressed in APP$^+$-*ob/ob* mice compared with other genotypes (Fig. 4*C*), suggesting that brain insulin signaling was disturbed in APP$^+$-*ob/ob* mice.

**Metabolic Features of APP$^+$-NSY Mice.** To further investigate the possible effect of Alzheimer-like pathology on diabetic phenotypes, we created another fusion mouse model between APP23 and diabetic NSY mice. We successfully generated such fusion mouse lines and selected three lines with mutually different brain Aβ levels (lines 16 and 17 and congenic mice; Fig. 5 *A* and *B*). All these fusion APP$^+$-NSY mice showed marked glucose intolerance in GTT compared with nondiabetic APP23 mice at 12 weeks of age (Fig. S5*C*). Although the APP$^+$-NSY mice showed mild obesity compared with the APP23 mice, their body weights were slightly, but significantly, decreased compared with those of the NSY mice, especially in the lines that have relatively high brain Aβ levels (line 16 and congenic mice) (Fig. S5*A*). There was no significant difference in food intake among these groups (Fig. S5*B*). To exclude the possible confounding effect of reduced body weights in APP$^+$-NSY mice on the results of GTT, we used body weight–matched mice groups (Fig. S5*D*). In these groups, APP$^+$-NSY (congenic) mice showed significantly severe glucose intolerance compared with NSY mice (Fig. 5*C*). Furthermore, we examined the correlation between the brain Aβ levels and the severity of glucose intolerance (Fig. 5*D*). We compared areas under the curve (AUCs) of glucose levels in GTT and levels of brain Aβ40 in the body weight–matched groups and observed a significant positive correlation between these parameters (Fig. 5*D*). In addition, we also found that the APP$^+$-NSY (congenic) mice exhibited severe insulin resistance compared with the NSY mice in insulin tolerance test (ITT) (Fig. 5*E*). These findings also support the possibility that amyloid pathology could adversely affect diabetic symptoms.

**Aggravation of Diabetes Induced Severe Memory Deficits in APP$^+$-NSY Mice.** To examine the effect of aggravated diabetic symptoms

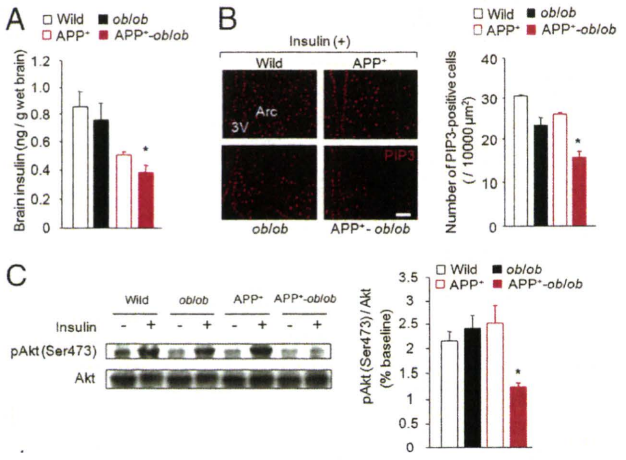


**Fig. 4.** Alteration in brain insulin signaling in APP+-*ob/ob* mice. (*A*) Quantification of brain insulin concentration by ELISA ($n$ = 5–9). (*B*) Insulin sensitivity in brain neurons. Insulin-stimulated (5.0 U/kg, i.p.) PIP3 formation in arcuate cells was assessed by immunostaining with anti-PIP3 antibody (*Left*). (Scale bar, 50 μm.) PIP3-positive cell number in arcuate nucleus of insulin-injected mice is shown in the graph (*Right*, $n$ = 3). (*C*) Immunoblot analysis of insulin-stimulated phosphorylation of Akt (pAkt) and total Akt in the brain (*Left*) and densitometric quantification of them (*Right*; $n$ = 3–4). *$P$ < 0.05 for APP+-*ob/ob* mice versus other genotypes. 3V, third ventricle; Arc, arcuate nucleus.

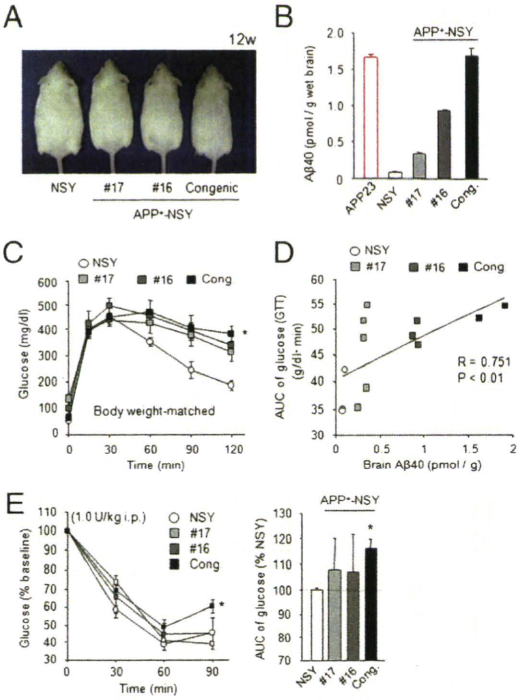


**Fig. 5.** Metabolic features of APP+-NSY mice. (*A*) Appearance of APP+-NSY mice (mice 16 and 17 and congenic mice) at 12 weeks. (*B*) Brain Aβ levels of each APP+-NSY mice lines (12-week-old age). (*C*) GTT in body weight–matched mice groups. Body weight–matched NSY and APP+-NSY mice were used for the experiment ($n$ = 3–5). *$P$ < 0.05 for APP+-NSY congenic mice compared with NSY mice. (*D*) Significant positive correlation between brain Aβ levels and glucose intolerance (AUC during GTT) in body weight–matched mice groups. $P$ < 0.01, Spearman rank test. (*E*) Blood glucose levels during ITT (1.0 U/kg, 12 weeks, $n$ = 4–7). *$P$ < 0.05 for APP+-NSY congenic mice compared with NSY mice. Cong., APP+-NSY congenic mice.

on cognitive function and brain Aβ levels in this model, NSY and APP+-NSY (line 16) mice were fed a high-fat (HF) or normal chow diet (ND) for 5 months (Fig. S6). HF feeding induced more weight gain (Fig. 6*A*), hyperglycemia (Fig. 6*B*), and glucose intolerance (Fig. 6*C*) than ND feeding. Compared with ND-fed APP+-NSY mice, HF-fed APP+-NSY mice showed increased learning impairment in the Morris water maze (Fig. 6*D*), although performance of HF-fed NSY mice was comparable to ND-fed NSY mice. In the visible-platform test, there were no differences in escape latency among all groups (Fig. 6*D*). Notably, HF feeding did not affect brain Aβ levels (Fig. 6*E*). In the brain of HF-fed APP+-NSY mice, increased cerebrovascular inflammation (IL-6–positive vessels; Fig. 6*F*) and insulin resistance in neuronal cells (Fig. 6*G*) were observed.

## Discussion

Although numerous epidemiological studies have demonstrated an increased risk of AD in patients with DM, the mechanistic interactions between AD and DM are still an enigma. With the use of established AD animal models that reflect the pathological conditions of both diseases, we demonstrated that (*i*) a diabetic condition enhanced cognitive dysfunction with cerebrovascular changes such as vascular inflammation and cerebral amyloid angiopathy, (*ii*) neuropathological changes were associated with impairment of brain insulin signaling, and (*iii*) amyloid pathology may adversely affect diabetic phenotypes.

One of the most important findings of the present study is that APP+-*ob/ob* mice demonstrated early onset of AD-like cognitive dysfunction at 8 weeks. It is noteworthy that, despite the early onset of cognitive dysfunction, APP+-*ob/ob* mice did not show an increase in brain Aβ burden compared with original APP+ mice (APP23). This phenomenon is consistent with clinical evidence that the burden of pathological hallmarks, including amyloid plaque, was not altered by the presence of DM (9, 10), although DM increased the risk of AD. In contrast, we observed severe amyloid deposition around brain microvessels in APP+-*ob/ob* mice. Furthermore, even before the development of cerebral amyloid angiopathy, APP+-*ob/ob* mice showed up-regulation of RAGE and inflammatory changes in the cerebral vasculature. HF-fed APP+-NSY mice also showed cognitive dysfunction associated with marked vascular inflammation, without an increase in brain Aβ. These results suggest the possibility that cerebrovascular alterations, but not brain parenchymal Aβ deposition, because of DM, might enhance cognitive dysfunction. Our previous study demonstrated that Aβ40 inhibited microvascular reendothelialization through the inhibition of phosphorylation of Akt, endothelial NOS, and PTEN (22). Impairment of vascular function such as vasodilation as a result of vascular inflammation or amyloid deposition might worsen the cognitive dysfunction in AD with DM. In addition, RAGE acts as a putative receptor for Aβ (13, 14) and induced an inflammatory response in the brain. Both AD and DM up-regulate RAGE expression in neuronal cells and the cerebral vasculature (13, 23). Our findings suggest that up-regulation of RAGE in the cerebral vasculature combined with the presence of Aβ in the brain of APP+-*ob/ob* mice may also cause cerebrovascular dysfunction, resulting in early onset of severe cognitive impairment. Considerable evidence now indicates the importance of cerebrovascular dysfunction in AD (11). Vascular dysregulation caused by the RAGE-Aβ interaction might be a possible explanation for the increased risk of AD in DM.

Neuroinflammation is believed to be one of the downstream events in the pathological cascade of AD (24). Aβ-induced inflammatory changes might contribute to neurodegeneration. In the present study, more prominent reactive gliosis was observed in the brain of APP+-*ob/ob* mice, despite the unaltered brain Aβ burden compared with APP+ mice. It might be possible that brain

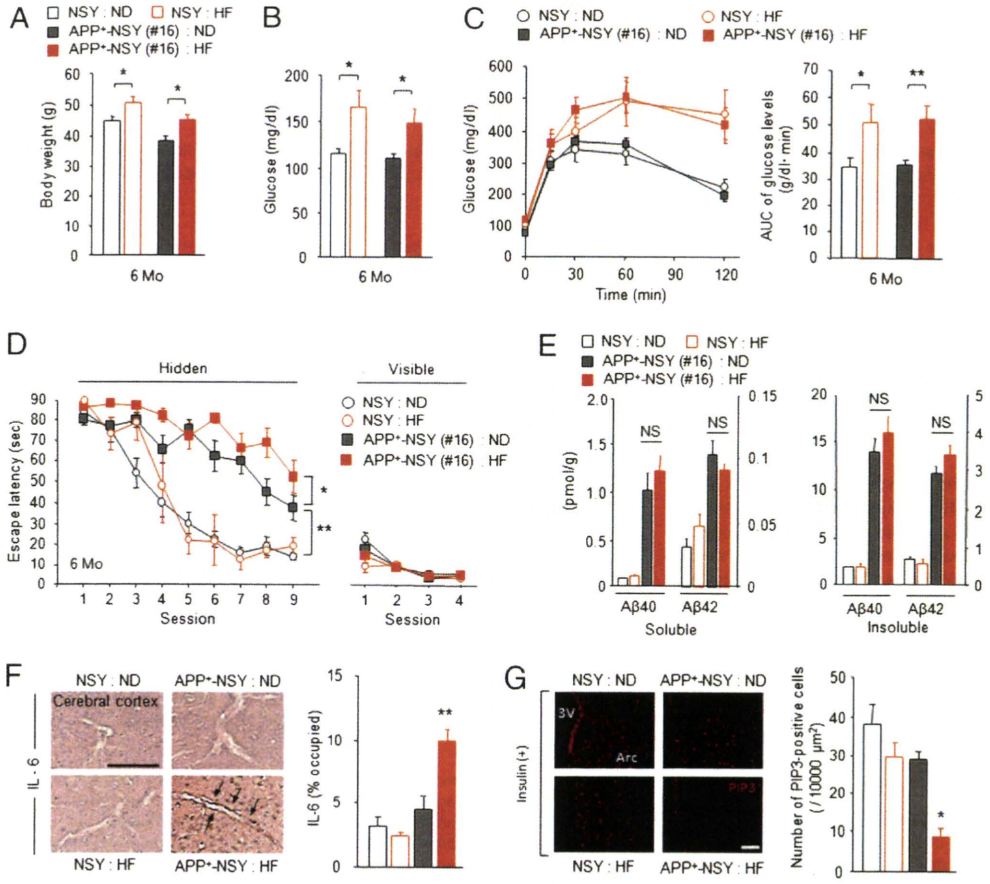


**Fig. 6.** Aggravation of diabetic conditions induce more severe memory deficits in APP+-NSY mice without an increase in brain Aβ load. (*A-C*) Five months of HF feeding aggravated diabetic phenotypes of APP+-NSY mice (mouse 16). One-month-old NSY and APP+-NSY mice were fed ND or HF diet for 5 months. (*A*) Body weight at 6 months of age ($n$ = 10–26). (*B*) Blood glucose levels in fed state ($n$ = 8–20). (*C*) Blood glucose levels during GTT ($n$ = 7–20 per group). $*P < 0.05$, $**P < 0.01$. (*D*) Morris water maze test at 6 months ($n$ = 3–15). $*P < 0.05$, $**P < 0.01$. (*E*) Quantification of brain Aβ40 and Aβ42 concentrations. Both soluble (Triton X-100 extract) and insoluble (guanidine extract) Aβ were measured ($n$ = 3–4). (*F*) IL-6–positive microvessels (cerebral cortex; *Left*) and quantitative image analysis (*Right*, $n$ = 4). (Scale bar, 100 μm.) $*P < 0.05$ for HF-fed APP+-NSY mice versus other groups. (*G*) Insulin sensitivity in brain neurons. Insulin-stimulated (5.0 U/kg, i.p.) PIP3 formation in arcuate cells was assessed by immunostaining ($n$ = 3). (Scale bar, 50 μm.) 3V, third ventricle; Arc, arcuate nucleus.

inflammation caused by DM might accelerate Alzheimer-like pathology in this model.

Another important finding of the present study is the impairment of insulin signaling in brain neurons of APP+-*ob/ob* mice. These data are consistent with reports that insulin resistance in the brain is implicated in the pathogenesis of AD (5, 8, 25). In this animal model, brain insulin level was significantly decreased in APP+-*ob/ob* mice. It has been reported that peripheral hyperinsulinemia could down-regulate brain insulin uptake at the blood–brain barrier (26). Combined with neuronal insulin resistance, brain insulin signaling may be disturbed in APP+-*ob/ob* mice. HF-fed APP+-NSY mice also showed insulin resistance in brain neurons, supporting the results of APP+-*ob/ob* mice. In this regard, restoration of brain insulin signaling could be an alternative therapeutic strategy for patients with AD, especially in those with DM.

In contrast, the increased severity of diabetic phenotype in APP+-*ob/ob* mice suggests that Alzheimer amyloid pathology may affect the pathogenesis of DM, as supported by some clinical studies (27, 28). Results of APP+-NSY mice also support the possible mutual interaction between AD and DM (Fig. 5). Importantly, it has become apparent that the brain plays a critical role in the regulation of energy metabolism in peripheral organs (29, 30). It might be possible that neuronal dysfunction induced by Aβ in the brain could impair glucose metabolism in peripheral organs. Another possibility could be the effect of circulating Aβ on peripheral organs. One recent report demonstrated that Aβ induced insulin resistance in cultured cells (31). Conversely, we recently found that the plasma Aβ level could be elevated by glucose loading or a fed state in Alzheimer transgenic mice (32). We also observed the same phenomenon in the present mouse model (Fig. S7). Increased plasma Aβ caused by hyperglycemia might worsen insulin resistance in peripheral organs. Of note, the limitation of these mice as an animal model of AD with DM should be recognized. In particular, as leptin regulated synaptic function and affected cognition and behavior (33), some of the phenotypes in APP+-*ob/ob* mice might result from the lack of leptin signaling. Although we obtained similar results using another mouse model (APP+-NSY mice), further studies would be necessary.

Here, we created Alzheimer mouse models with early onset of cognitive dysfunction. Cerebrovascular changes such as inflammation and alteration in brain insulin signaling might play a pivotal role in the early onset of AD. These established diabetic AD mouse models could provide insights to develop a strategy for the prevention and treatment of AD. The possibility of mutual interaction between AD and DM has clinically important implications.

## Materials and Methods

**Animal Models.** APP+-*ob/ob* mice were produced by cross-breeding APP23 mice and *ob/ob* mice (Charles River). Male heterozygous APP23 (APP+) mice were cross-bred with female heterozygous *ob/+* mice to generate APP+-*ob/+* and *ob/+* founder mice. We then intercrossed these mice to obtain APP+-*ob/ob*, APP+, *ob/ob*, and WT littermate mice. All mice were on the same genetic background (C57BL/6J). APP+-NSY mice were generated using the pronuclear microinjection technique. See *SI Materials and Methods* for details of APP+-NSY mice. We used only male mice for the present study.

**Animal Experiments.** All animal experiments were performed in compliance with the Guidelines for the Care and Use of Laboratory Animals of the Osaka University School of Medicine. Animals were maintained at room temperature (25 ± 2 °C) under a standard 12-h/12-h light-dark cycle, with free access to water and ND or HF diet. See *SI Materials and Methods* for details of measurement of food intake, water consumption, and urine volume.

**Metabolic Measurements.** Blood glucose and plasma insulin determinations were performed in fasted (for 16 h) and randomly fed states. See *SI Materials and Methods* for details of blood glucose and plasma insulin measurement, GTT, and ITT. Metabolic parameters were measured at approximately the same time (early light phase).

**Western Blotting.** Tissue samples were lysed and processed for immunoblot analysis as described in *SI Materials and Methods*.

**Behavioral Analysis.** Hippocampus-dependent learning and memory function were investigated with the Morris water maze test, as detailed in *SI Materials and Methods*. To assess basal activity of animals, the open field test was carried out (*SI Materials and Methods*).

**Measurement of Aβ.** Fresh-frozen mouse brain was serially homogenized into detergent-soluble and guanidine HCl-soluble fractions, as detailed in *SI Materials and Methods*. The amounts of Aβ X-40 and Aβ X-42 in each fraction were determined by BNT-77/BA-27 and BNT-77/BC-05 sandwich ELISA (Wako Pure Chemical), respectively, according to the manufacturer's instructions.

**Immunohistochemical Staining.** Mouse brains were paraformaldehyde fixed, paraffin-embedded, and cut into sections 10 μm thick. For immunodetection of amyloid plaque, we used anti-Aβ (6E10) antibody coupled with secondary horseradish peroxidase-conjugated antibody (Vectastain ABC-kit; Vector Laboratories) and diaminobenzidine reaction. We also stained the sections with rabbit anti-GFAP antibody (1:80, G9269; Sigma), goat anti-ChAT polyclonal antibody (1:100, AB144P; Chemicon), rabbit anti-RAGE polyclonal antibody (1:100, ab3611; Abcam), rat anti-CD31 (PECAM-1) monoclonal antibody (1:50; BD Pharmingen), goat anti-IL-6 polyclonal antibody (1:100, sc1265; Santa Cruz Biotechnology), and goat anti-TNF-α polyclonal antibody (1:100, sc1351; Santa Cruz Biotechnology), and visualized immunoreactions using a fluorescent secondary antibody or horseradish peroxidase–conjugated antibody with diaminobenzidine reaction.

**Image Analysis.** A detailed description of image analysis is provided in the *SI Materials and Methods*.

**Measurement of Brain Insulin Level.** The amount of insulin was determined by ELISA (Morinaga Seikagaku) in a fasted state. See *SI Materials and Methods* for details.

**In Vivo Insulin Stimulation Assay.** We assessed insulin sensitivity of each organ (muscle, liver, and brain) using an in vivo insulin stimulation assay as described previously (21, 34). See also *SI Materials and Methods* for details.

**Isolation of Brain Microvessels and Immunohistochemical Staining.** Brain microvessels were isolated and characterized as described previously (19). A detailed description of these techniques is also provided in *SI Materials and Methods*.

**Statistical Analysis.** All data are expressed as mean ± SEM. Two-group comparisons were performed by Student *t* test. Comparison of means among three or more groups was performed by ANOVA followed by Tukey-Kramer multiple range test. *P* values less than 0.05 were considered significant.

**ACKNOWLEDGMENTS.** We thank M. Staufenbiel (Novartis Institutes for BioMedical Research, Basel, Switzerland) for providing APP23 mice and Y. Ueda (Molecular Endocrinology, Graduate School of Medicine, Osaka University, Osaka, Japan) and T. Fujisawa (Department of Geriatric Medicine, Osaka University, Osaka, Japan) for helpful discussion. This work was supported in part by grants-in-aid from Japan Promotion of Science; the Japanese Ministry of Education, Culture, Sports, Science and Technology (R.M., N.S.); and the Japan Science and Technology Agency (N.S.).



1. Flier JS (2004) Obesity wars: molecular progress confronts an expanding epidemic. *Cell* 116:337–350.
2. Maher PA, Schubert DR (2009) Metabolic links between diabetes and Alzheimer's disease. *Expert Rev Neurother* 9:617–630.
3. Ott A, et al. (1999) Diabetes mellitus and the risk of dementia: The Rotterdam Study. *Neurology* 53:1937–1942.
4. Hardy J, Selkoe DJ (2002) The amyloid hypothesis of Alzheimer's disease: progress and problems on the road to therapeutics. *Science* 297:353–356.
5. Gasparini L, Netzer WJ, Greengard P, Xu H (2002) Does insulin dysfunction play a role in Alzheimer's disease? *Trends Pharmacol Sci* 23:288–293.
6. Phiel CJ, Wilson CA, Lee VM, Klein PS (2003) GSK-3alpha regulates production of Alzheimer's disease amyloid-beta peptides. *Nature* 423:435–439.
7. Qiu WQ, Folstein MF (2006) Insulin, insulin-degrading enzyme and amyloid-beta peptide in Alzheimer's disease: review and hypothesis. *Neurobiol Aging* 27:190–198.
8. Ho L, et al. (2004) Diet-induced insulin resistance promotes amyloidosis in a transgenic mouse model of Alzheimer's disease. *FASEB J* 18:902–904.
9. Alafuzoff I, Aho L, Helisalmi S, Mannermaa A, Soininen H (2009) Beta-amyloid deposition in brains of subjects with diabetes. *Neuropathol Appl Neurobiol* 35:60–68.
10. Arvanitakis Z, et al. (2006) Diabetes is related to cerebral infarction but not to AD pathology in older persons. *Neurology* 67:1960–1965.
11. Iadecola C (2004) Neurovascular regulation in the normal brain and in Alzheimer's disease. *Nat Rev Neurosci* 5:347–360.
12. Nogueira-Machado JA, Chaves MM (2008) From hyperglycemia to AGE-RAGE interaction on the cell surface: a dangerous metabolic route for diabetic patients. *Expert Opin Ther Targets* 12:871–882.
13. Deane R, et al. (2003) RAGE mediates amyloid-beta peptide transport across the blood-brain barrier and accumulation in brain. *Nat Med* 9:907–913.
14. Arancio O, et al. (2004) RAGE potentiates Abeta-induced perturbation of neuronal function in transgenic mice. *EMBO J* 23:4096–4105.
15. Sturchler-Pierrat C, et al. (1997) Two amyloid precursor protein transgenic mouse models with Alzheimer disease-like pathology. *Proc Natl Acad Sci USA* 94: 13287–13292.
16. Ueda H, et al. (2000) Age-dependent changes in phenotypes and candidate gene analysis in a polygenic animal model of type II diabetes mellitus; NSY mouse. *Diabetologia* 43:932–938.
17. Smith EE, Greenberg SM (2009) Beta-amyloid, blood vessels, and brain function. *Stroke* 40:2601–2606.
18. Beckman JA, Creager MA, Libby P (2002) Diabetes and atherosclerosis: epidemiology, pathophysiology, and management. *JAMA* 287:2570–2581.
19. Zhou J, Ando H, Macova M, Dou J, Saavedra JM (2005) Angiotensin II AT1 receptor blockade abolishes brain microvascular inflammation and heat shock protein responses in hypertensive rats. *J Cereb Blood Flow Metab* 25:878–886.
20. Chiu SL, Chen CM, Cline HT (2008) Insulin receptor signaling regulates synapse number, dendritic plasticity, and circuit function in vivo. *Neuron* 58:708–719.
21. Schubert M, et al. (2004) Role for neuronal insulin resistance in neurodegenerative diseases. *Proc Natl Acad Sci USA* 101:3100–3105.
22. Hayashi S, et al. (2009) Alzheimer disease-associated peptide, amyloid beta40, inhibits vascular regeneration with induction of endothelial autophagy. *Arterioscler Thromb Vasc Biol* 29:1909–1915.
23. Liu LP, et al. (2009) Upregulation of RAGE at the blood-brain barrier in streptozotocin-induced diabetic mice. *Synapse* 63:636–642.
24. Wyss-Coray T (2006) Inflammation in Alzheimer disease: driving force, bystander or beneficial response? *Nat Med* 12:1005–1015.
25. Zhao WQ, et al. (2009) Insulin receptor dysfunction impairs cellular clearance of neurotoxic oligomeric abeta. *J Biol Chem* 284:18742–18753.
26. Craft S (2005) Insulin resistance syndrome and Alzheimer's disease: age- and obesity-related effects on memory, amyloid, and inflammation. *Neurobiol Aging* 26 (Suppl 1): 65–69.
27. Craft S, Zallen G, Baker LD (1992) Glucose and memory in mild senile dementia of the Alzheimer type. *J Clin Exp Neuropsychol* 14:253–267.
28. Fujisawa Y, Sasaki K, Akiyama K (1991) Increased insulin levels after OGTT load in peripheral blood and cerebrospinal fluid of patients with dementia of Alzheimer type. *Biol Psychiatry* 30:1219–1228.
29. Schwartz MW, Porte D, Jr. (2005) Diabetes, obesity, and the brain. *Science* 307: 375–379.
30. Uno K, et al. (2006) Neuronal pathway from the liver modulates energy expenditure and systemic insulin sensitivity. *Science* 312:1656–1659.
31. Zhao WQ, et al. (2008) Amyloid beta oligomers induce impairment of neuronal insulin receptors. *FASEB J* 22:246–260.
32. Takeda S, et al. (2009) Elevation of plasma beta-amyloid level by glucose loading in Alzheimer mouse models. *Biochem Biophys Res Commun* 385:193–197.
33. Morrison CD (2009) Leptin signaling in brain: A link between nutrition and cognition? *Biochim Biophys Acta* 1792:401–408.
34. Niswender KD, et al. (2003) Insulin activation of phosphatidylinositol 3-kinase in the hypothalamic arcuate nucleus: a key mediator of insulin-induced anorexia. *Diabetes* 52:227–231.